Large eddy simulation of turbulent natural convection in concentric horizontal annuli

Yasutomi Miki
Cooperative Research Center, Kitami Institute of Technology, Kitami, Japan

Kenji Fukuda
Department of Nuclear Engineering, Faculty of Engineering, Kyushu University, Fukuoka, Japan

Noboru Taniguchi
Department of Energy Conversion, Interdisciplinary Graduate School of Engineering Sciences, Kyushu University, Kasuga, Japan

The large eddy simulation (LES) based on subgrid modeling has been applied to turbulent natural convection in concentric horizontal annuli with a heated inner and a cooled outer cylinder. The unsteady three-dimensional Boussinesq approximated equations were solved using the explicit finite-difference method. The highest Rayleigh number solution obtained was 1.18×10^9. The time-averaged temperature distributions and the mean Nusselt numbers obtained here are in reasonable agreement with the experimental results of other researchers. The effects of the number of grid cells and the Smagorinsky constant on the time-averaged temperature distributions and turbulence properties are also discussed.

Keywords: turbulent natural convection; concentric horizontal annuli; large eddy simulation; subgrid scale model; Smagorinsky constant; finite-differencing

Introduction

Natural convection in concentric horizontal cylindrical annuli kept at constant surface temperatures is a classical laboratory problem and has been studied by many researchers experimentally and analytically because of its interesting flow patterns and of its engineering applications in technologies such as solar concentrators, inert-gas insulated electrical cables, and horizontal pressurized heavy water reactors (PHWRs). The previous research was comprehensively reviewed by Gebhart et al. (1988) and Bishop and McLeod (1989). The problem has been studied experimentally by Beckmann (1931), Kraussold (1934), Liu et al. (1961), Lis (1966), and Grigull and Hauf (1966). There have been several correlations presented for the average heat transfer between cylinders. Several researchers have also presented the temperature distributions and the qualitative descriptions of principally laminar flow using photographs and optical methods. Powe et al. (1969) have presented the detailed descriptions and the photographs of stable laminar and oscillating laminar flow in air. Kuehn and Goldstein (1978) have obtained the temperature distributions and the local heat transfer coefficients by optical methods for nitrogen for Rayleigh numbers based on gap width up to 8×10^7. More recently Bishop (1988) has presented the time-averaged temperature distributions and the overall heat transfer rates for Rayleigh numbers up to 1.8×10^9, a constant Prandtl number of 0.688, and a diameter ratio of 3.36. McLeod and Bishop (1989) have performed an experimental study of the natural convection of helium between isothermal concentric cylinders at cryogenic temperatures and have presented the overall heat transfer rates and the time-averaged temperature distributions for Rayleigh numbers of 8×10^6–2×10^9 and expansion numbers of 0.25–1.0. On the other hand, most of the analytical works were limited to Rayleigh numbers less than around 10^5. Actually, the only results reported in the literature for Rayleigh numbers greater than 5×10^5 are from Farouk and Guceri (1982) and Fukuda et al. (1990). Farouk and Guceri (1982) used the high-Reynolds-number k-ε model for the two-dimensional (2-D) turbulent natural convection in concentric horizontal annuli for Rayleigh numbers up to 10^7.

In a previous paper (Fukuda et al., 1990), we have studied the validity and the limit of the numerical simulation using no turbulence model for natural convection in concentric horizontal annuli at moderate Rayleigh numbers up to 6.0×10^5. It was found that the numerical simulation using no turbulence model replicated the time-averaged temperature distributions and the mean Nusselt number satisfactorily except for the cases of relatively high Rayleigh numbers, where it tended toward too large turbulence levels. Due to the limitation of the number of grid cells for the finite-difference method, it was important to evaluate the effect of the number of grid cells and their width to confirm the validity of the results. Also, at higher Rayleigh numbers, it seemed to be, after all, inevitable to include some model

Address reprint requests to Professor Miki at Cooperative Research Center, Kitami Institute of Technology, Kitami 090, Japan.

Received 23 April 1992; accepted 10 October 1992

for the subgrid scale turbulent Reynolds stress and the corresponding turbulent heat flux.

Therefore, in the present study we have tested the applicability of the LES based on subgrid modeling to natural convection in concentric horizontal annuli for Rayleigh numbers up to 1.18×10^9. To this end, we have evaluated the effect of the number of grid cells and the Smagorinsky constant on the time-averaged temperature distributions and the turbulence properties by comparing the results from the numerical simulation using no turbulence model and the experimental results of other researchers.

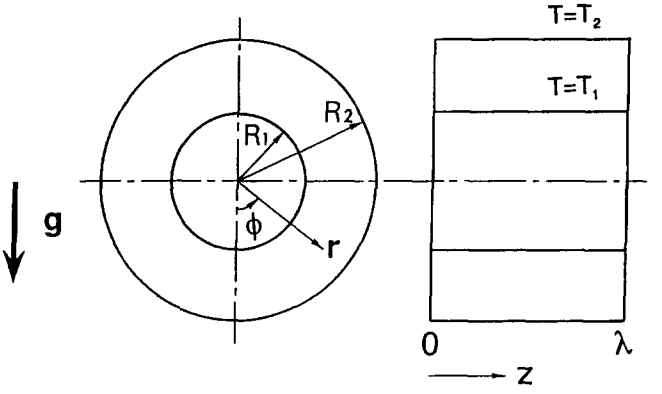

Figure 1 Problem configuration and coordinate system

Model equations and solution procedure

LES flow equations

The configuration to be studied is shown in Figure 1. Concentric horizontal cylindrical annuli are heated on the inner cylinder surface and cooled on the outer one. The LES equations are formed by filtering the continuity, Boussinesq-approximated Navier–Stokes and energy equations with the well-known Top-Hat filter (Moin and Kim 1982). Here, the higher-order correlation terms or the Leonard and the cross-terms are neglected. These equations are put into dimensionless form using the scale L for length, L^2/α for time, α/L for velocity, $\rho(\alpha/L)^2$ for pressure, and $(T_1 - T_2)$ for temperature. The resultant dimensionless equations of mass, motion, and energy are as follows.

Conservation of mass

$$\frac{\partial \overline{u_i}}{\partial x_i} = 0 \tag{1a}$$

Conservation of momentum

$$\frac{\partial \overline{u_i}}{\partial t} + \frac{\partial (\overline{u_i}\overline{u_j})}{\partial x_j} = -\frac{\partial \overline{p}}{\partial x_i} + \frac{\partial}{\partial x_j}\left(-\overline{u_i' u_j'} + \mathrm{Pr}\frac{\partial \overline{u_i}}{\partial x_j}\right) + \mathrm{Pr}\mathrm{Ra}_L \overline{T}\mathbf{e} \tag{1b}$$

Conservation of energy

$$\frac{\partial \overline{T}}{\partial t} + \frac{\partial (\overline{u_i}\overline{T})}{\partial x_j} = \frac{\partial}{\partial x_j}\left(-\overline{u_i' T'} + \frac{\partial \overline{T}}{\partial x_j}\right) \tag{1c}$$

Notation

C_k	Model constant for Equation 4
C_S	Smagorinsky constant
$\mathbf{e}$	Unit vector of the direction of the gravitational force, $(\cos\phi, -\sin\phi, 0)$
E_{GS}	Grid scale (GS) energy
E_{SGS}	Subgrid scale (SGS) energy
f_d	Damping function
F_{rr}	One-dimensional energy spectrum
g	Acceleration of gravity
K_M	Turbulent viscosity
K_T	Turbulent conductivity
k_z	Wave number in z-direction
L	Gap width of the annulus, $R_2 - R_1$
Nu_1, Nu_2	Mean Nusselt number at the inner and the outer cylinder surfaces respectively, defined in Equation 6
Nu_m	Arithmetic average value of Nu_1 and Nu_2
p	Dimensionless fluid pressure
Pr	Molecular Prandtl Number, ν/α
Pr_t	SGS turbulent Prandtl number, K_M/K_T
r	Dimensionless radial coordinate, $(r - R_1)/(R_2 - R_1)$
R_1, R_2	Radii of the inner and outer cylinders, respectively
Ra_L	Rayleigh number based on the gap width, $g\beta(T_1 - T_2)L^3/\alpha\nu$
S_{ij}	Strain tensor
t	Dimensionless time
T	Dimensionless fluid temperature
u_i or (u_r, u_ϕ, u_z)	Dimensionless fluid velocity
x_i or (r, ϕ, z)	Dimensionless space coordinate
y_w	Distance from the nearest wall divided by L
y^+	Dimensionless distance from the nearest wall, $y_w\sqrt{(\partial \bar{u}_\phi/\partial r)_w}/\sqrt{\mathrm{Pr}}$
z	Dimensionless axial coordinate z/L

Greek symbols

α	Thermal diffusivity
β	Coefficient of thermal expansion
δ_{ij}	Kronecker delta
λ	Periodicity length
ν	Kinematic viscosity
ρ	Mean density
ϕ	Angular coordinate measured from downward vertical axis
Δ_f	Filter width, $(\Delta_r\Delta_\phi\Delta_z)^{1/3}$

Subscripts

1	Inner cylinder
2	Outer cylinder
i	i-direction
r	Radial direction
w	Value at the wall
z	Axial direction
ϕ	Angular direction
$\langle\ \rangle$	Time-averaged value
$''$	Fluctuation value from time-averaged value
$\bar{}$	Filtered or grid scale (GS) value
$'$	Subgrid scales (SGS) value

In Equations 1a–1c, u_i, p, and T are the dimensionless velocity, pressure, and temperature, respectively. ($\bar{}$) and ($'$) are a filtered or grid scale (GS) value and a subgrid scale (SGS) value, respectively. **e** is a unit vector of the direction of the gravitational force, $(\cos\phi, -\sin\phi, 0)$. And Pr and Ra_L are the molecular Prandtl number and the Rayleigh number based on the gap width L, respectively.

Modeling of the subgrid correlation terms

From a dimensional analysis and the production (including a buoyancy contribution)-dissipation equilibrium arguments, the SGS Reynolds stress term and the SGS turbulent heat flux terms are modeled. We assume the subgrid turbulence to be isotropic, so the eddy viscosity/conductivity approximation is applied. Here, the following form, first presented by Smagorinsky (1963) and modified by Eidson (1985) is used:

$$\overline{u_i'u_j'} - \tfrac{1}{3}\delta_{ij}\overline{u_k'u_k'} = -K_M\bar{S}_{ij} \tag{2a}$$

$$\overline{u_i'T'} = -K_T\frac{\partial\bar{T}}{\partial x_i} \tag{2b}$$

$$\bar{S} = 2(\bar{S}_{ij}\bar{S}_{ij})^{1/2} \tag{2c}$$

and

$$\bar{S}_{ij} = \frac{1}{2}\left(\frac{\partial\bar{u}_i}{\partial x_j} + \frac{\partial\bar{u}_j}{\partial x_i}\right) \tag{2d}$$

where K_M and K_T are the eddy viscosity/conductivity, respectively. And K_M is defined by the following equation (including the buoyancy-production correction):

$$K_M = \frac{(C_S\Delta_f)^2}{2^{1/2}}\left(\bar{S}^2 - \frac{1}{\mathrm{Pr}_t}\mathrm{PrRa}_L\mathbf{e}\frac{\partial\bar{T}}{\partial x_j}\right)^{1/2},\quad K_T = \frac{K_M}{\mathrm{Pr}_t} \tag{3}$$

where Δ_f, C_S, and Pr_t are the filter width, the Smagorinsky constant, and the SGS turbulent Prandtl number, respectively. The values of 1/3–1/1.195 have been chosen in the previous numerical studies. A value of 1/2.5 was selected for the numerical study of the turbulent Rayleigh–Benard problem (Eidson 1985). Here, a value of 1/1.2 proposed by Yoshizawa (1983) is used for Pr_t. The value of C_S will be discussed later.

In order to make Equation 3 compatible with the nonslip boundary condition, the value of Δ_f is multiplied to the Van Driest exponential damping function $f_d = 1 - \exp(-y^+/25)$, where y^+ is the distance from the nearest wall in dimensionless wall units (Moin and Kim 1982; Tsai and Leslie 1990).

The SGS turbulent energy E_{SGS} is given by

$$E_{SGS} = K_M^2/(C_k\Delta_f)^2 \tag{4}$$

where $C_k = 0.09$ with the assumption of homogeneous turbulence at subgrid levels (Lilly 1966).

Boundary conditions

The above equations are subject to the following boundary conditions:

$$\overline{u_r} = \overline{u_\phi} = \overline{u_z} = 0 \qquad (r = R_1, R_2)$$

$$\bar{T} = 1 \qquad (r = R_1)$$

$$\bar{T} = 0 \qquad (r = R_2)$$

$$\frac{\partial\bar{p}}{\partial r} = -\mathrm{Pr}\left\{\frac{\partial}{\partial r}\left(\frac{\partial\overline{u_z}}{\partial z}\right) + \frac{1}{r^2}\frac{\partial}{\partial r}\left(\frac{\partial\overline{u_\phi}}{\partial\phi}\right)\right\} - \mathrm{PrRa}\bar{T}\cos\phi \tag{5}$$

$$(r = R_1, R_2)$$

$$\xi(r, 0, z) = \xi(r, 2\pi, z)$$

$$\xi(r, \phi, 0) = \xi(r, \phi, \lambda) \qquad (\text{where } \xi = \overline{u_i}, \bar{T}, \bar{p})$$

which represent the nonslip boundary condition on the cylinder surfaces and the periodic boundary condition in the z-direction.

Solution procedure

The explicit finite-difference scheme as in Williams (1969) and Grotzbach (1982) is used. The second-order accurate Adams–Bashforth scheme is used for temporal derivatives, and the second-order accurate central differencing is used for spatial ones. Uniform grid lengths are chosen in the ϕ- and z-directions and nonuniform in the r-direction. The dependent variables are staggered on the numerical grid. The Poisson equation for the pressure is solved by a discrete Fourier transform (DFT) method. The time step Δt is taken in the range of $5.0 \times 10^{-8} < \Delta t < 1.0 \times 10^{-5}$.

Case specifications

Several numerical simulations with different Rayleigh numbers, different Prandtl numbers, different aspect ratios, different grids, different periodicity lengths, and different Smagorinsky constants were carried out (Table 1). Cases 1–4, 5, 6, 7, and 8–12 were chosen for direct comparison with the experimental results of Kuehn and Goldstein (1978), Bishop (1988), Liu et al. (1961), Kuehn and Goldstein (1978), and McLeod and Bishop (1989), respectively. For Cases 1–6 and 12, a value of $C_S = 0$ was used. For the other cases, nonzero values of C_S

Table 1 Case specifications

Case	Ra_L	Pr	R_2/R_1	$N_r \times N_\phi \times N_z$	λ/L	Δt	C_S	Reference
1	2.51×10^6	0.731	2.60	24 × 96 × 32	2.8	5.0×10^{-6}	0.0	Kuehn et al. (1978)
2	2.51×10^6	0.731	2.60	36 × 96 × 32	2.8	2.5×10^{-6}	0.0	Kuehn et al. (1978)
3	2.51×10^6	0.731	2.60	36 × 96 × 64	2.8	2.5×10^{-6}	0.0	Kuehn et al. (1978)
4	2.51×10^6	0.731	2.60	36 × 96 × 64	5.6	2.5×10^{-6}	0.0	Kuehn et al. (1978)
5	1.31×10^7	0.688	3.36	36 × 96 × 64	2.8	2.5×10^{-6}	0.0	Bishop (1988)
6	1.72×10^7	7.830	2.50	36 × 96 × 64	2.8	2.5×10^{-6}	0.0	Liu et al. (1961)
7	2.51×10^6	0.731	2.60	36 × 96 × 64	5.6	2.5×10^{-6}	0.1	Kuehn et al. (1978)
8	1.22×10^7	0.688	4.85	36 × 96 × 64	5.6	2.5×10^{-6}	0.1	McLeod et al. (1989)
9	1.35×10^8	0.688	4.85	36 × 96 × 64	5.6	5.0×10^{-7}	0.1	McLeod et al. (1989)
10	1.18×10^9	0.688	4.85	36 × 96 × 64	5.6	2.5×10^{-7}	0.1	McLeod et al. (1989)
11	1.18×10^9	0.688	4.85	36 × 96 × 64	5.6	2.5×10^{-7}	0.2	McLeod et al. (1989)
12	1.18×10^9	0.688	4.85	36 × 96 × 64	5.6	2.5×10^{-8}	0.0	McLeod et al. (1989)

were used. For Cases 1–3, with the same other parameters, different grids were used. Cases 3 and 4 differ from each other in their periodicity length. The Rayleigh numbers specified for Cases 5 and 6 are higher than those of Cases 1–4. The Rayleigh numbers specified for Cases 10–12 are also higher than those of Cases 7–9. Cases 10–12, which are different in the value of C_S, were taken to confirm the high-Rayleigh-number simulation of this problem.

Comparison of results and discussion

Starting from the solution obtained for a smaller Rayleigh number, the governing equations were integrated forward in time until the numerical solutions reached statistically steady states. The steady states were also identified by approximate agreement of both mean Nusselt numbers at the outer and inner cylinder surfaces, expressed as follows:

$$\mathrm{Nu}_1 = \frac{1}{2\pi}\int_0^{\lambda}\int_0^{2\pi} R_1 \ln(R_1/R_2)\left(\frac{\partial \overline{T}}{\partial r}\right)_{r=R_1} d\phi\, dz$$

$$\mathrm{Nu}_2 = \frac{1}{2\pi}\int_0^{\lambda}\int_0^{2\pi} R_2 \ln(R_1/R_2)\left(\frac{\partial \overline{T}}{\partial r}\right)_{r=R_2} d\phi\, dz \qquad (6)$$

Next, in order to obtain better statistical samples, the governing equations were further integrated in time. For each case, the simulations were considered to be complete when the time-averaged turbulence quantities became stationary. Sixty samples storaged per 60 time steps were used for time averaging. In order to compare the results with those of the previous laboratory experiments, the results given in all figures represent the axially averaged values. Both mean Nusselt numbers at the outer and inner cylinder surfaces were within the relative error of 1 percent, excluding the simulation with the highest Rayleigh number (1.3 percent for Case 10), showing a good heat balance between both cylinders. The CPU time consumed on a FACOM VP200 was about 0.7 seconds per time step, which resulted in a total CPU time of 12.5 hours, for example, for Case 10.

Comparison between the simulations using no turbulence model and experimental results

First, the cases of $C_S = 0$ (corresponding to the numerical simulation using no turbulence model) are considered, and the results are compared with experimental results (Cases 1–6). In Figure 2 are shown the time-averaged temperature distributions compared with the experimental results. For Case 3, good agreement is obtained, but for Case 6 there are small discrepancies. Since the temperature difference between both cylinders is large in the experiments, Rayleigh numbers in the experiments strongly depend on the characteristic temperature at which physical properties are defined. Bishop (1988), in common with the present paper, adopted a volume-averaged temperature as the characteristic temperature; however, it gives a higher Rayleigh number than does the choice of the temperature nearer to the inner cylinder surface. Thus, the reason for the discrepancy for Case 6 might be twofold; the number of grid cells in the simulations using no turbulence model is not enough and/or the characteristic temperature to calculate Rayleigh numbers should be the one nearer to the inner cylinder surface.

Effect of Smagorinsky constant C_S

For high Rayleigh numbers, it seems to be necessary to introduce a turbulence model for the SGS Reynolds stress

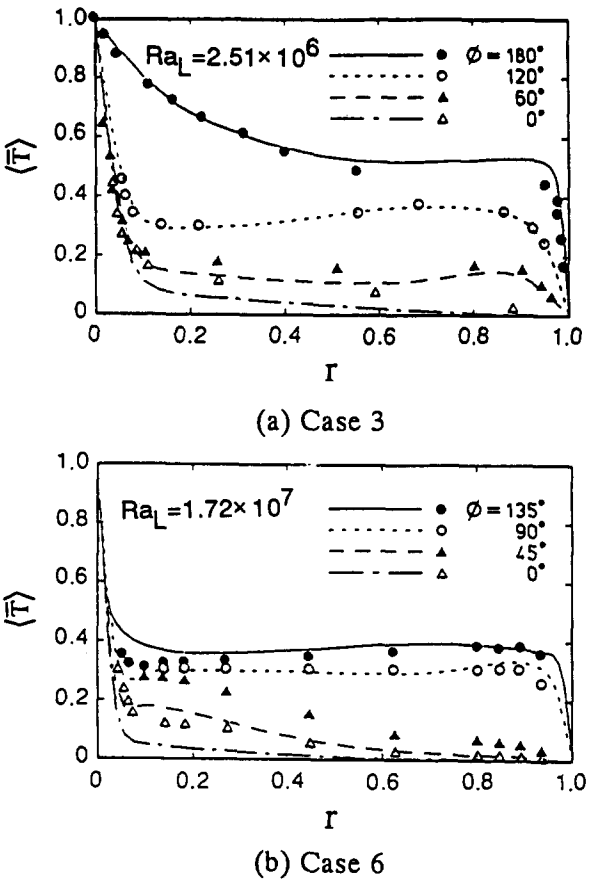

Figure 2 Time-averaged temperature distribution by the simulations using no turbulence model; (a) lines: simulation (Case 3); symbols: Kuehn and Goldstein (1978); (b) lines: simulation (Case 6); symbols: Liu et al. (1961).

and the SGS turbulent heat flux. In LES it is important to choose a value of the Smagorinsky constant C_S appropriately. Values of this parameter from the representative numerical studies as well as the theoretical estimates by Lilly (1966) and Yoshizawa (1983) are shown in Table 2, excluding

Table 2 Values of C_S from several studies

Values of C_S	Reference
Theory	
0.18–0.22	Lilly (1966)
0.081	Yoshizawa (1983)
Isotropic turbulence	
0.21	Kwak (1975)
0.24	Shaanan (1975)
0.17–0.19	Clark (1979)
0.19–0.24	Mansour et al. (1979)
0.14–0.16	McMillan and Ferziger (1979)
Channel flow	
0.1	Deardorff (1970)
0.1	Horiuchi (1982)
0.065	Moin and Kim (1982)
0.14	Kaneda and Leslie (1983)
0.1	Tsai and Leslie (1990)
Atmospheric convection	
0.21 (unstable case)	Deardorff (1972)
0.13 (neutral case)	Deardorff (1972)
0.14	Schemm and Lipps (1976)
Rayleigh–Benard convection	
0.21	Eidson (1985)

the values from the studies of the LES by the volume-averaging procedure and the most recent studies. Values of 0.14–0.24 were used for the numerical studies of the homogeneous isotropic flow, and values of 0.065–0.14 were chosen for the studies of the turbulent channel flow. The values of 0.13–0.21 were selected for the numerical study of atmospheric convection (Deardorff 1972; Schemm and Lipps 1976) and $C_S = 0.21$ for the study of the turbulent Rayleigh–Benard problem (Eidson 1985). Here, we have examined the effect of varying C_S to identify its appropriate value. Figure 3 shows the time-averaged 1-D energy spectra of the velocity fluctuation in the r-direction at $r = 0.4$. For the case of the highest Rayleigh number ($= 1.18 \times 10^9$), the energy spectra for $C_S = 0.1$ (Case 10) and $C_S = 0.2$ (Case 11) are compared. It is clearly shown that the slope of the energy spectrum becomes steeper as C_S increases, indicating that more energy is dissipated with larger C_S. For the case of $C_S = 0$ (Case 12), we could not obtain a steady solution even if Δt is reduced to 1/10 of those for Cases 10 and 11. The energy spectrum for Case 12 in Figure 3 is an instantaneous one, and notable amounts of energy with high wave numbers are accumulated at the top of the annulus. Thus, the numerical accumulation of energy at high wave numbers is the penalty resulting from not using any turbulence model; the rate of energy dissipation is controlled by changing C_S.

The time-averaged velocity and the time-averaged temperature distributions for Cases 10 and 11 are shown in Figure 4. It is found that the effect of C_S on the time-averaged distributions are relatively small. However, the corresponding rms distributions of velocity and temperature fluctuations are much affected by changing C_S (see Figure 5). Thus, by applying the LES technique we may obtain a reasonable time-averaged distribution without much consideration of C_S, which is confirmed later by comparing the results with experiments, but the turbulence properties are very sensitive to C_S.

It is found that for the case of $C_S = 0.1$ (Case 10), E_{SGS} is only 5–7 percent of E_{GS} and that this small amount of energy dissipation avoids the accumulation of energy at high wave numbers. On the other hand, when $C_S = 0.2$ (Case 11), E_{SGS}/E_{GS} attains 8 as its maximum value, which is unphysical and seems to be beyond the limit of applicability of the LES technique. We thus used 0.1 thereafter.

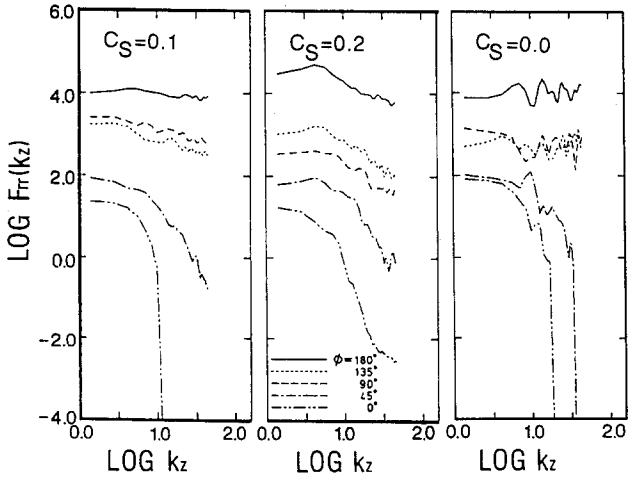

Figure 3 Effect of C_S on time-averaged 1-D energy spectra of the velocity fluctuation by LES; Case 10: $C_S = 0.1$; Case 11: $C_S = 0.2$; Case 12: $C_S = 0.0$

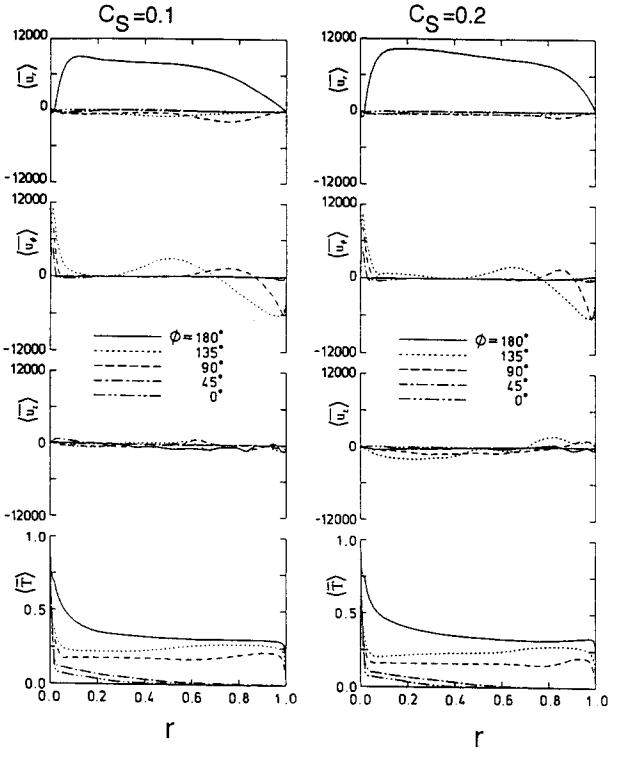

Figure 4 Effect of C_S on time-averaged velocity and temperature distribution by LES; Case 10: $C_S = 0.1$; Case 11: $C_S = 0.2$

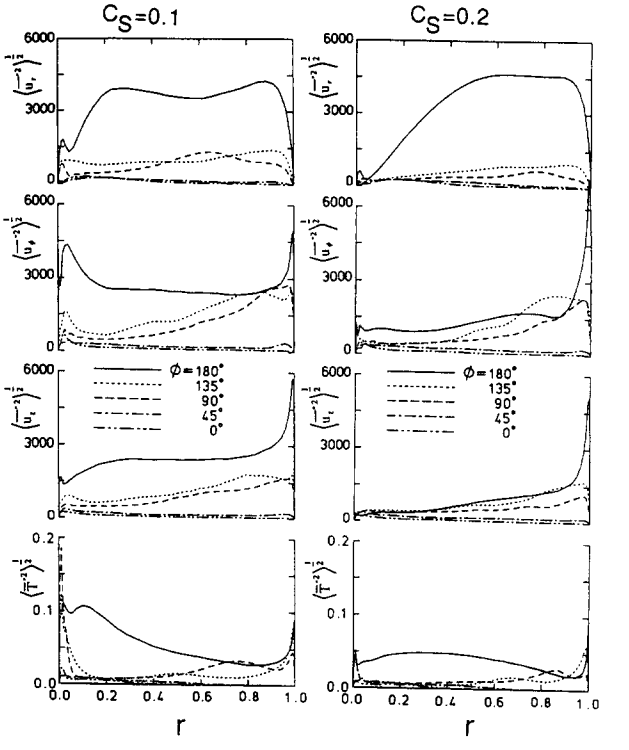

Figure 5 Effect of C_S on rms of velocity and temperature fluctuations by LES; Case 10: $C_S = 0.1$; Case 11: $C_S = 0.2$

Comparison between LES and experimental results

The time-averaged temperature distributions obtained by LES for Cases 8 and 10 are compared with those of experiments (McLeod and Bishop 1989) in Figure 6. It is

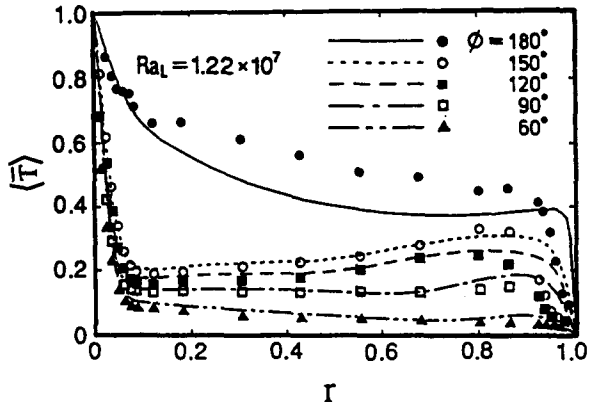

(a) Case 8

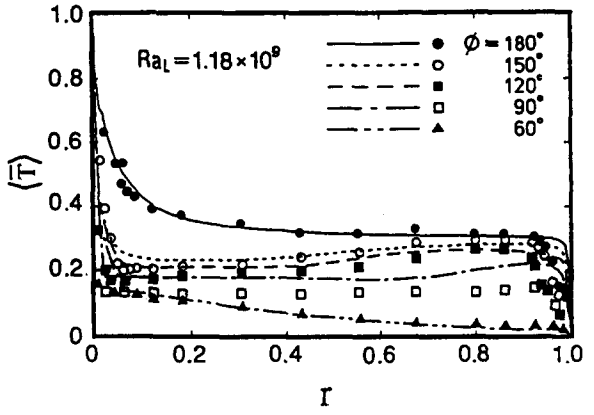

(b) Case 10

Figure 6 Time-averaged temperature distribution by LES; (a) lines: simulation (Case 8); symbols: McLeod and Bishop (1989); (b) lines: simulation (Case 10); symbols: McLeod and Bishop (1989)

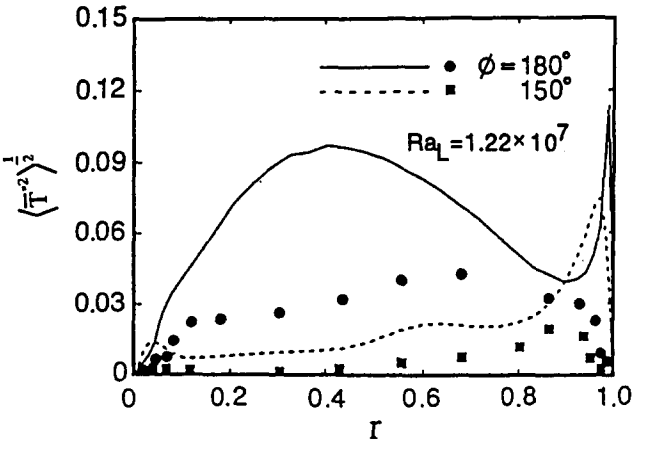

(a) Case 8

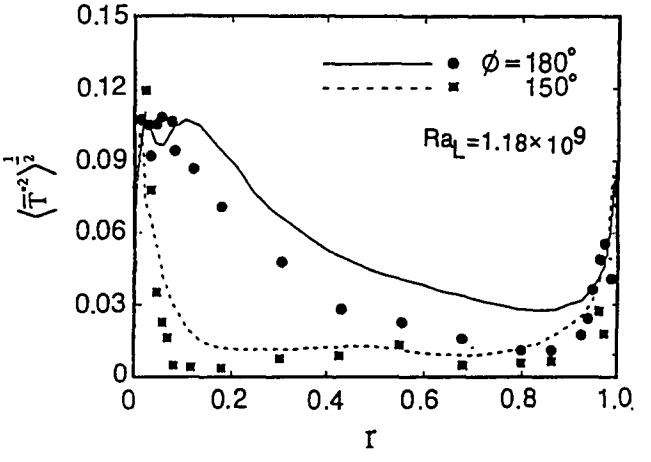

(b) Case 10

Figure 7 Rms of temperature fluctuations by LES; (a) lines: simulation (Case 8); symbols: McLeod and Bishop (1989); (b) lines: simulation (Case 10); symbols: McLeod and Bishop (1989)

found that LES predicts the experimental results quite well, except for small discrepancies for Case 8, where the simulation predicts the lower temperatures at the top of the annulus, and in Cases 8 and 10, where the simulations give steeper slopes in the boundary layer on the outer cylinder surface.

In Figure 7 are shown rms distributions of temperature fluctuations. Discrepancies are rather large, especially near the top of the annulus in Case 8. However, by looking closer in the figures, it is found that the peak value of the fluctuation moves from the core to the inner cylinder surface side as the Rayleigh number increases.

Heat transfer results

Figure 8 shows the values of the mean Nusselt number Nu_m, defined as the arithmetic average value of Nu_1 and Nu_2, derived from the numerical simulations and experimental results. The solid line shows the results from the correlation equation of Itoh et al. (1970). The values of Nu_m are in good agreement with those of other experiments and with the correlation equation of Itoh et al. (1970), except for the case of the highest Rayleigh number. But the results from McLeod and Bishop (1989) are slightly larger than those from the present simulations and the correlation equation

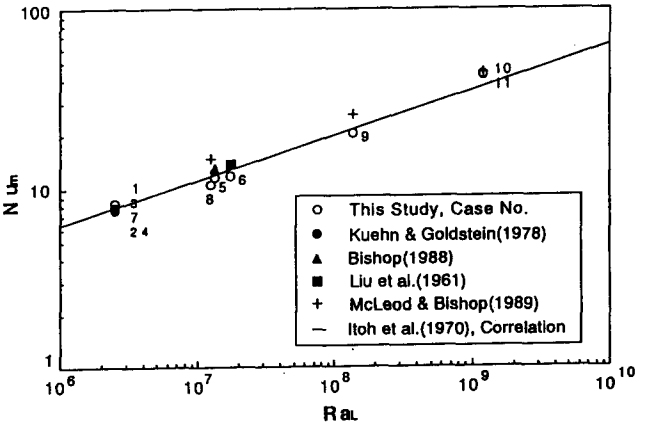

Figure 8 The mean Nusselt numbers versus Rayleigh number; ○: simulations; ●: Kuehn and Goldstein (1978); ▲: Bishop (1988); ■: Liu et al. (1961); +: McLeod and Bishop (1989); solid line: Itoh et al. (1970)'s corresponding equation

of Itoh et al. (1970). Farouk and Guceri (1982) have presented turbulent flow results for Rayleigh numbers of 10^6–10^7, but did not report the values of Nu_m. The need for further work on natural convection heat transfer of extremely high Rayleigh numbers is evident.

Conclusion

Numerical simulations of turbulent natural convection in concentric horizontal annuli have been conducted using the LES technique, and the results have been compared with several laboratory experiments. The overall results seem to demonstrate that the LES technique can be used to predict this problem. The following are the major observations and conclusions of this study.

(1) For the numerical simulations using no turbulence model, time-averaged temperature distributions are reasonably predicted, provided that the number of grid cells is sufficient;
(2) because of the restriction on the number of grid cells, there is a limit in the Rayleigh number beyond which the numerical simulations using no turbulence model are not valid or the calculation itself is not possible;
(3) the additional terms associated with the subgrid scale model in LES dissipate energy at high wave numbers, and the amount of dissipation depends strongly on the Smagorinsky constant, C_S; and
(4) the values of mean Nusselt number are in good agreement with those of the experiments of other researchers and of the correlation equation of Itoh et al. (1970), except for the case of the highest Rayleigh number. But the simulation slightly underpredicts the mean Nusselt number compared with McLeod and Bishop (1989).

Acknowledgment

This work was carried out with financial support by the Ministry of Education, Japan from research Grant No. 01550181, type C and by Japan Atomic Energy Research Institute (JAERI) under Grant No. 90155. The numerical work was conducted using the supercomputers in the Computing Center of Kyushu University and JAERI.

References

Beckmann, W. 1931. Die Wärmenüberstrangung in zylindrischen Grasshichten bei natürlicher Konvektion. *Forschung*, **2**, Bd.5, 165–178

Bishop, E. H. 1988. Heat transfer by natural convection of helium between horizontal isothermal concentric cylinders at cryogenic temperature. *J. Heat Transfer*, **110**, 109–114

Bishop, E. H. 1990. Private communication

Clark, R. A., Ferziger, J. H., and Reynolds, W. C. 1979. Evaluation of subgrid-scale turbulence models using a fully simulated turbulent flow. *J. Fluid Mech.*, **91**, 1–16

Deardorff, J. W. 1970. A numerical study of three-dimensional turbulent channel flow at large Reynolds numbers. *J. Fluid Mech.*, **41**, 453–480

Deardorff, J. W. 1972. Numerical investigation of neutral and unstable planetary boundary layers. *J. Atmos. Sci.*, **29**, 91–115

Eidson, T. M. 1985. Numerical simulation of the turbulent Rayleigh–Benard problem using subgrid modeling. *J. Fluid Mech.*, **158**, 245–268

Farouk, B. and Guceri, S. I. 1982. Laminar and turbulent natural convection in the annulus between horizontal concentric cylinders. *J. Heat Transfer*, **104**, 631–636

Fukuda, K., Miki, Y., and Hasegawa, S. 1990. Analytical and experimental study on turbulent natural convection in a horizontal annulus. *Int. J. Heat Mass Transfer*, **33**, 629–639

Gebhart, B., Jaluria, Y., Mahajan, R. L., and Sammakia, B. 1988. *Buoyancy-Induced Flows and Transport*. Springer-Verlag, 764–770

Grigull, U. and Hauf, W. 1966. Natural convection in horizontal transfer in simple and obstructed horizontal annuli. *Proc. Third Int. Heat Conf.*, Vol. 2, 182–195

Grotzbach, G. 1982. Direct numerical simulation of laminar and turbulent Benard convection. *J. Fluid Mech.*, **119**, 27–53

Horiuchi, K. 1982. Study of incompressible turbulent channel flow by large eddy simulation. *Theor. Appl. Mech.*, **31**, 407–427

Itoh, M., Fujita, T., Nishiwaki, N., and Hirata, M. 1970. A new method of correlating heat transfer coefficients for natural convection in horizontal cylindrical annuli. *Int. J. Heat Mass Transfer*, **13**, 1364–1368

Kaneda, Y. and Leslie, D. C. 1983. Tests of subgrid models in the near-wall region using represented velocity fields. *J. Fluid Mech.*, **132**, 349–373

Kraussold, H. 1934. Wärmeabgabe von zylindrischen flüssigkeitsschichten bei natürlicher konvektion. *Forsch. Geb. IngWes.*, **5**, 186–191

Kuehn, T. H. and Goldstein, R. J. 1978. An experimental study of natural convection heat transfer in concentric and eccentric horizontal cylindrical annuli. *J. Heat Transfer*, **100**, 635–640

Kwak, D. 1975. Three-dimensional time dependent computation of turbulent flow. Ph.D thesis, Dept. of Mechanical Engineering, Stanford University, Stanford, CA

Lilly, D. K. 1966. The representation of small-scale turbulence in numerical simulation experiments. *IBM Sci. Comput. Symp.*, **14**, 195–210

Lis, J. 1966. Experimental investigation of natural convection heat transfer in simple and obstructed horizontal annuli. *Proc. Third Int. Heat Conf.*, Vol. 2, 196–204

Liu, C. Y., Muller, W. K., and Landis, F. 1961. Natural convection heat transfer in long horizontal cylindrical annuli. *Int. Dev. Heat Transfer*, **5**, 976–984

Mansour, N. N., Moin, P., Reynolds, W. C., and Ferziger, J. H. 1979. Improved methods for large eddy simulations of turbulence. In F. Durst et al. (eds.), *Turbulent Shear Flows I*. 386–401

McLeod, A. E. and Bishop, E. H. 1989. Turbulent natural convection of gases in horizontal cylindrical annuli at cryogenic temperatures. *Int. J. Heat Mass Transfer*, **32**, 1967–1978

McMillan, O. J. and Ferziger, J. H. 1979. Direct testing of subgrid-scale models. *AIAA J.*, **17**, 1340–1346

Moin, P. and Kim, J. 1982. Numerical investigation of turbulent channel flow. *J. Fluid Mech.*, **118**, 314–377

Powe, R. E., Carley, C. T., and Bishop, E. H. 1969. Free convection flow patterns in cylindrical annuli. *J. Heat Transfer*, **91**, 310–314

Schemm, C. E. and Lipps, F. B. 1976. Some results from a simplified three-dimensional numerical model of atmospheric turbulence. *J. Atmos. Sci.*, **33**, 1021–1041

Shaanan, S. 1975. Numerical simulation of turbulence in the presence of shear. Ph.D. thesis, Dept. of Mechanical Engineering, Stanford University, Stanford, CA

Smagorinsky, J. 1963. General circulation experiments with the primitive equations. *Mon. Weather Rev.*, **91**, 99–115

Tsai, H. M. and Leslie, D. C. 1990. Large eddy simulation of a developing turbulent boundary layer at a low Reynolds number. *Int. J. Numer. Methods Fluids*, **10**(5), 519–555

Yoshizawa, A. 1983. A statistical theory of thermally-driven turbulent shear flows, with the derivation of a subgrid model. *J. Phys. Soc. J.*, **52**, 1194–1205

Williams, G. P. 1969. Numerical integration of the three-dimensional Navier–Stokes equations for incompressible flow. *J. Fluid Mech.*, **37**, 727–750